Struct Multidisc Optim (2006) 32: 263–275
DOI 10.1007/s00158-006-0037-7

RESEARCH PAPER

Søren Halkjær · Ole Sigmund · Jakob S. Jensen

Maximizing band gaps in plate structures

Received: 6 January 2006 / Revised manuscript received: 27 April 2006 / Published online: 20 July 2006

Abstract Band gaps, i.e., frequency ranges in which waves cannot propagate, can be found in elastic structures for which there is a certain periodic modulation of the material properties or structure. In this paper, we maximize the band gap size for bending waves in a Mindlin plate. We analyze an infinite periodic plate using Bloch theory, which conveniently reduces the maximization problem to that of a single base cell. Secondly, we construct a finite periodic plate using a number of the optimized base cells in a postprocessed version. The dynamic properties of the finite plate are investigated theoretically and experimentally and the issue of finite size effects is addressed.

Keywords Elastic band gaps · Topology optimization · Experimental investigation · Dynamics

1 Introduction

Infinite plates with a periodic modulation of the material properties or voids, also called sonic crystals (SC), may prohibit propagation of elastic waves in certain frequency intervals, commonly referred to as the elastic (or phononic) band gap phenomenon (Sigalas and Economou 1994). This can, in turn, lead to very low vibration levels of finite structures exposed to harmonic loads at these frequencies. Such a phenomenon can be exploited effectively within important practical areas, such as vibration insulation of sensitive equipment from surrounding vibrations or vibration insulation of noisy machinery from the surroundings.

The phenomenon raises a number of interesting and important design problems such as how to design crystals with maximum band gap sizes and how large should the crystals be in terms of number of periodic repetitions to maintain the desired band gap properties. Typically, such design problems are treated by introducing a number of design variables and by defining a cost function to measure the performance of the design, thus resulting in a minimization problem. Methods of solutions include genetic algorithms, other global heuristic approaches, and gradient-based algorithms. The heuristic approaches are most suitable for problems with a small number of design variables and nonsmooth objective functions. Gradient-based topology optimization has gained increasing popularity during the last decade (see Bendsøe and Sigmund 2003 for an overview). An important reason is the possibility of working with a large number of design variables and, in principle, the unlimited design freedom.

In this work, we use the topology optimization method to design an infinite single-material Mindlin plate with maximized band gap size for bending waves. Then the vibrational response of a corresponding finite structure is investigated. This is an extension of an earlier work (Halkjær et al. 2005) where we optimized an infinite bimaterial Mindlin plate consisting of a base material (PMMA) and an inclusion material (aluminum) with respect to maximum relative band gap size for bending waves. Other works on topology optimization of phononic band gaps include the study of Sigmund and Jensen (2003) who were the first to topology optimize sonic band gap structures and Diaz et al. (2005) who optimized the band gap properties of grillage structures. Sigalas et al. (2005) reviews the area of SC.

The topology optimization method has likewise received increasing attention in the closely related research area of photonic crystals due to the potentially large application possibilities for using these in optical circuits (Jensen and Sigmund 2004; Borel et al. 2004). Band gap optimization of

S. Halkjær · O. Sigmund · J.S. Jensen (✉)
Section for Solid Mechanics, Department of Mechanical Engineering, Technical University of Denmark, Nils Koppels Allé 404, 2800 Lyngby, Denmark
Tel.: +45-45254280
Fax: +45-45931475
e-mail: jsj@mek.dtu.dk

Present Address:
S. Halkjær
OTICON A/S, Kongebakken 9, 2765 Smørum, Denmark
Tel.: +45-45254297
Fax: +45-45931475
e-mail: sha@oticon.dk

O. Sigmund
Tel.: +45-45254256
Fax: +45-45931475
e:mail: sigmund@mek.dtu.dk

infinite structures are found in, e.g., Cox and Dobson (1999) and Kao et al. (2005).

2 Theory

Classical (thin) plate theory for bending waves becomes inaccurate when the wavelength is less than five to ten times the plate thickness (Mindlin 1951). Anticipating wavelengths of this order or smaller, we use Mindlin plate theory (moderately thick plates) in our bending wave study.

2.1 The infinite periodic plate

For bending waves in up to moderately thick plates, the governing equations are (Graff 1991; Leissa 1993):

$$\begin{aligned}\frac{\rho d^3}{12}\frac{d^2\Theta_x}{dt^2} &- \frac{\partial}{\partial x}\left(D\frac{\partial\Theta_x}{\partial x}\right) - \frac{\partial}{\partial y}\left((1-\nu)\frac{D}{2}\frac{\partial\Theta_x}{\partial y}\right)\\ &- \frac{\partial}{\partial x}\left(\nu D\frac{\partial\Theta_y}{\partial y}\right) - \frac{\partial}{\partial y}\left((1-\nu)\frac{D}{2}\frac{\partial\Theta_y}{\partial x}\right)\\ &- Gkd\left(\frac{\partial w}{\partial x} - \Theta_x\right) = 0 \end{aligned} \tag{1}$$

$$\begin{aligned}\frac{\rho d^3}{12}\frac{d^2\Theta_y}{dt^2} &- \frac{\partial}{\partial y}\left(\nu D\frac{\partial\Theta_x}{\partial x}\right) - \frac{\partial}{\partial x}\left((1-\nu)\frac{D}{2}\frac{\partial\Theta_x}{\partial y}\right)\\ &- \frac{\partial}{\partial x}\left((1-\nu)\frac{D}{2}\frac{\partial\Theta_y}{\partial x}\right) - \frac{\partial}{\partial y}\left(D\frac{\partial\Theta_y}{\partial y}\right)\\ &- Gkd\left(\frac{\partial w}{\partial y} - \Theta_y\right) = 0 \end{aligned} \tag{2}$$

$$\begin{aligned}\rho d\frac{d^2w}{dt^2} &- \frac{\partial}{\partial x}\left(Gkd\frac{\partial w}{\partial x}\right) - \frac{\partial}{\partial y}\left(Gkd\frac{\partial w}{\partial y}\right)\\ &+ \frac{\partial}{\partial x}\left(Gkd\Theta_x\right) + \frac{\partial}{\partial y}\left(Gkd\Theta_y\right) = 0 \end{aligned} \tag{3}$$

Here, d is the plate thickness, ρ the mass density, ν the Poisson's ratio, G the shear modulus, $D \equiv Ed^3/(1-\nu^2)$ the flexural rigidity, E the Young's modulus, and k the shear correction factor (here, $k = 1/1.2$). The variable w denotes the deflection normal to the plane of the plate, Θ_x denotes the angle between the x-axis and a cross section in the yz-plane, and similarly for Θ_y.

We assume that the plate is infinite and periodic (a crystal), described by a base cell and two lattice vectors $\mathbf{R}_1$ and $\mathbf{R}_2$. For a plane wave traveling with wave vector, $\mathbf{k}$ Bloch theory (Matthews and Walker 1964) states that

$$w(\mathbf{r}+\mathbf{R}_j) = \mathrm{e}^{\mathrm{i}\mathbf{R}_j\cdot\mathbf{k}}w(\mathbf{r}), \qquad j = 1,2 \tag{4}$$

with similar relations for the other two variables Θ_x and Θ_y. Condition (4) can be enforced directly in the governing equations (1–3) (c.f. Cox and Dobson 1999). Here, we use a simpler implementation of the boundary conditions (4) imposed directly in the finite element (FE) equations with a standard penalization technique.

In the analysis, we assume time-harmonic displacements with angular frequency ω. A FE discretization of (1–3) on the base cell domain using (4) results in the standard generalized eigenvalue problem formulation:

$$(\mathbf{K} - \omega^2\mathbf{M})\mathbf{u} = \mathbf{0} \tag{5}$$

where $\mathbf{K}$ and $\mathbf{M}$ are the usual stiffness and mass matrices, respectively. The vector $\mathbf{u}$ contains all the discretized nodal values of the original continuous variables w, Θ_x, and Θ_y.

The dispersion relation $\omega = \omega(\mathbf{k})$ is the solution to (5). For infinite homogeneous plates, all frequencies are allowed, i.e., each frequency corresponds to at least one real wave vector. However, frequency band gaps may be introduced in the corresponding dispersion plot when voids are introduced in the base cell. Mathematically, these gaps consist of frequencies with corresponding complex wave vectors in the dispersion relation. From (4) it is seen that the amplitude of such a wave decreases exponentially in space. It is these (relative) gaps that we wish to study and maximize in the following subsection.

2.2 The optimization problem

The present optimization problem concerns optimized distribution of a single (base) material[1] with respect to maximum frequency band gap size. We introduce element-wise constant design variables

$$0 \le \zeta_e \le 1, \ e = 1, \ldots, \ N. \tag{6}$$

where N denotes the total number of elements. Letting ϱ_e denote an element-wise property (such as Young's modulus or the mass density), we define the material interpolation scheme as

$$\varrho_e = (1-\zeta_e)\varrho_0 + \zeta_e\varrho_1 \tag{7}$$

where subscript 0 refers to the properties of the (nearly) void material and subscript 1 refers to the properties of the chosen solid material. We use nonzero properties of the void material to ensure positive definite stiffness and mass matrices. It is well-known in static compliance problems concerning the optimized distribution of a single material (Bendsøe and Sigmund 2003) that raising the design variable in (7) to a power p larger than 1 is typically necessary to force the design variable to one of its extreme values to obtain a design amenable to fabrication. A study similar to the present (Sigmund and Jensen 2003) but concerned with *planar* wave propagation showed that one obtains high contrast designs without the need for penalization. In our experience with the bending wave case presented in this paper, however, we found out that gray elements do appear. Unfortunately, the usual solid isotropic material with penalization (SIMP) scheme assumes a volume constraint in order to work because it is based

[1] Chosen a priori

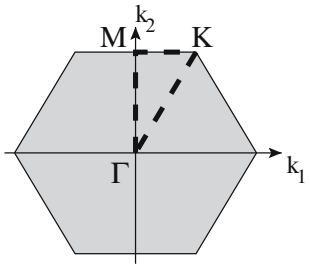

Fig. 1 Irreducible Brillouin zone for a rhombic base cell

on making the use of intermediate densities uneconomical. Hence, when optimizing band gaps, the SIMP scheme will not work. Instead, we apply an explicit mesh-independent penalization scheme as an extra constraint as suggested by Borrvall and Petersson (2001).

With the purpose of maximizing the relative band gap size, the topology optimization problem is formulated by defining a cost function Φ (Sigmund and Jensen 2003) equal to the relative band gap size between band j and band $j+1$

$$\max_{\zeta\in[0,1]^N} : \Phi(\boldsymbol{\zeta}) = \frac{\Delta\omega}{\omega_0} = 2\frac{\min\limits_{\mathbf{k}} \omega_{j+1} - \max\limits_{\mathbf{k}} \omega_j}{\min\limits_{\mathbf{k}} \omega_{j+1} + \max\limits_{\mathbf{k}} \omega_j} \tag{8}$$

where the band gap size is found as the difference between the lowest point on the upper band $j+1$ and the highest point on the lower band j. The wave vector $\mathbf{k}$ should take any value within the first Brillouin zone for a rhombic base cell (see Fig. 1). Due to the symmetries in the rhombic cell, the search area can be further reduced to the triangular area indicated in the figure. Furthermore, it is commonly accepted that it is sufficient to search only on the edges of the zone.

A fixed base cell geometry is chosen to reduce the overall optimization problem. The particular choice of geometry is based on the result of a previous similar study by Halkjær et al. (2005), indicating that a rhombic shape is superior to a rectangular shape with respect to large relative band gap sizes. For the same reason, size and thickness as well as the material constituent are also chosen a priori and kept fixed during the topology optimization. Apart from the unit cell geometry and Poisson's ratio, these variables mostly scale and translate the frequency bands and thus are not very important for the resulting topology itself.

In our case, the topology optimization problem is now completely described by (5–8). The analysis is performed using the commercial FE program COMSOL, which can be called from a MATLAB script that includes the optimization routine method of moving asymptotes (Svanberg 1987). Three thousand six hundred rhombic first-order elements were used in the FE analysis.

An optimized design using (8) with $j=1$ (maximization of the relative gap size between the first and second band) is shown in Fig. 2a with Polycarbonate (Young's modulus E_1=2.3 GPa, mass density ρ_1=1,200 kg/m^3, and Poisson's ratio ν_1=0.35) chosen as the base material. The dimensions of the base cell are length (0.033 m) and thickness (0.003 m). The weak material has the material properties

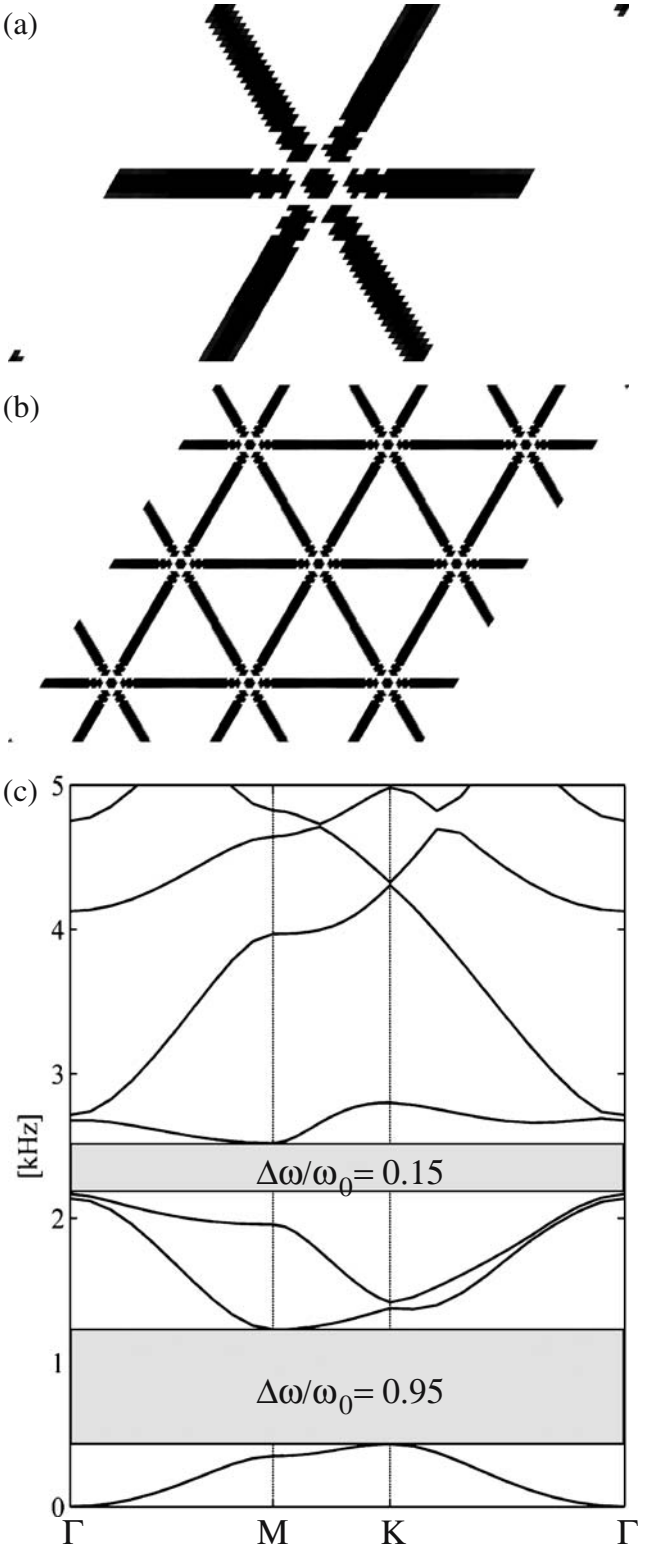

Fig. 2 **a** Optimized base cell design using the cost function (8). **b** A repeated structure consisting of 3×3 base cells. **c** The corresponding dispersion plot which shows eigenfrequencies as function of wave vector values indicated by the *dashed* line in Fig. 1

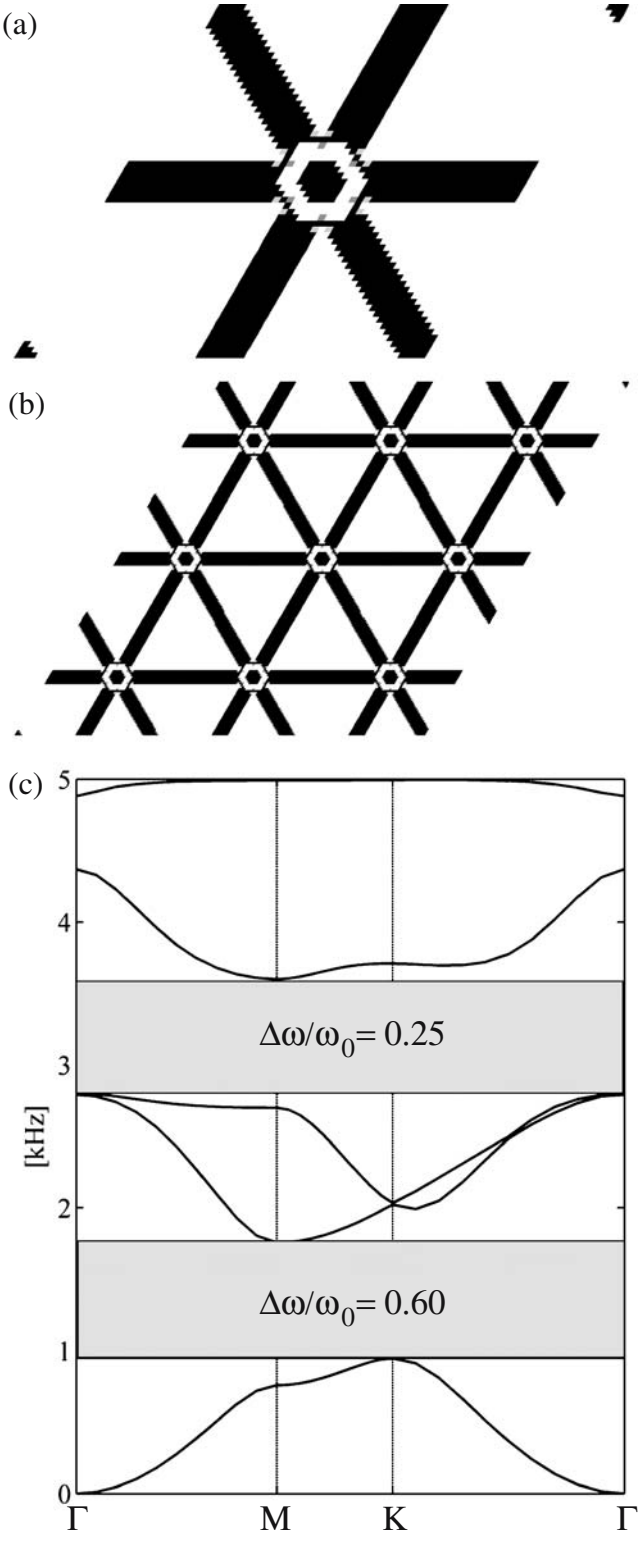

Fig. 3 **a** Optimized base cell design using the cost function (9). **b** A repeated structure consisting of 3×3 base cells. **c** The corresponding dispersion plot

E_0=0.0023 GPa, ρ_0=12 kg/m^3, and $\nu_0 = 0.35$. The optimized structure is seen to be degenerate with disconnected beams and masses. The corresponding dispersion plot that gives the frequency of the propagating modes for the wave vectors on the triangular path in Fig. 1 is shown at the bottom of the figure. The figure depicts the maximized band gap (highlighted and with relative size 0.95) and a second band gap (relative size 0.15) between the third and fourth bands. The background for the degeneracy of the structure is simple to explain. Basically, we are trying to maximize the difference between the first and the second eigenfrequency for the plate. This is obtained by minimizing the first eigenfrequency (i.e., minimizing the structural integrity) and maximizing the second eigenfrequency. To obtain a better structure we need to modify the objective function.

The cost function in (8) favors large gaps for low frequencies. This is successfully accomplished with the disconnected structure in Fig. 2. However, the static stiffness of the structure is very low, making the design useless in practice. To remedy this problem one could try to open the gap for higher frequencies by modifying the objective function. Simply removing the mean gap frequency ω_0 from the denominator is not sufficient but if we choose to multiply the gap $\Delta\omega$ by ω_0^2, the optimized gap is moved up in the frequency range resulting in designs with sufficient rigidity. Thus, the new cost function is

$$\max_{\zeta\in[0,1]^N} : \Phi(\zeta) = \Delta\omega\omega_0^2 = (\min_{\mathbf{k}} \omega_{j+1} - \max_{\mathbf{k}} \omega_j) \times \frac{1}{4}(\min_{\mathbf{k}} \omega_{j+1} + \max_{\mathbf{k}} \omega_j)^2 \quad (9)$$

An optimized design resulting from the use of (9) again with $j = 1$ and the same geometry as above is seen in Fig. 3a. In this case the beams are connected with a circular rim. A circular area is enclosed by the rim, making the circular center area work as a softly extended internal resonator. Figure 3c shows the corresponding dispersion plot with the maximized band gap (highlighted and with relative size 0.6) and the second band gap (with relative size 0.25). It is seen from the dispersion plot that the frequency bands (and the gaps) are positioned at larger values compared to the previous case, as expected, ensuring better structural integrity.

Although it has smaller relative band gap sizes, we have chosen to proceed with the latter design due to its better abilities of supporting objects. We use a postprocessed version to make the resulting design more robust and easier to fabricate. The circular area and rim were replaced with beam segments, such that the base cell consists of crossing beams. The postprocessed design is shown in Fig. 4 (right) and illustrates that the final design consists of triangular holes in a base material. The equivalence is obvious from Fig. 4 (left), which shows one base cell shifted half a period compared to Fig. 3a. The performed postprocessing was found to have a quantitative effect on the relative band gap sizes, as the postprocessed design exhibits a larger relative size of the second band gap than the first band gap.

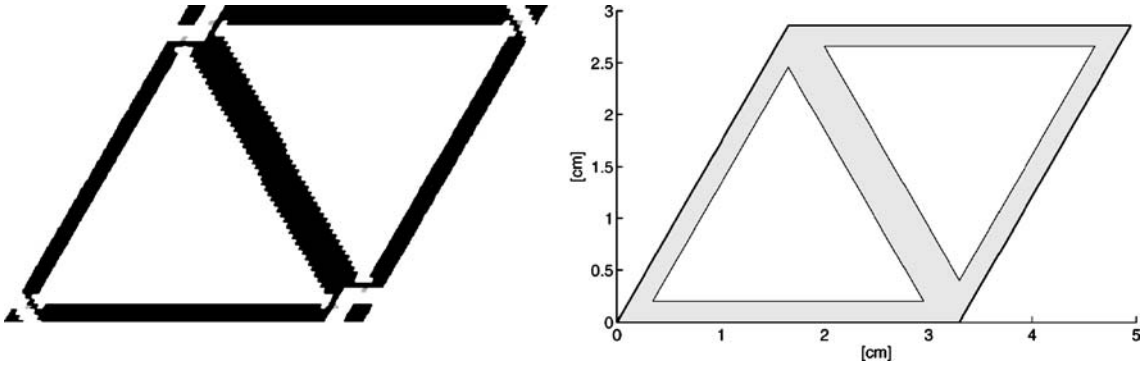

Fig. 4 *Left*: optimized base cell from Fig. 3b. *Right*: the postprocessed version of the optimized base cell

Based on preliminary studies, the dimensions of the base cell were selected according to the following considerations. For experimental reasons, it was the goal to create and maximize a relative band gap around 5 kHz. As noted previously, the actual positions of the band gaps can be adjusted by proper selection of base cell dimensions. As base material we choose PolyCarbonate (as it is easier to create holes in it) with a thickness of 3 mm (the material are properties listed in Table 1), such that holes can be fabricated with enough precision. With these choices it was found that centering the second band gap around 5 kHz resulted in a larger relative band gap size than centering the first band gap around 5 kHz. The resulting dimensions are shown in Fig. 4 (right) with base cell length equal to 3.3 cm and diagonal wall thickness equal to 0.41 cm. The corresponding dispersion plot is shown in Fig. 5b. The two band gaps are shown, the first just below 2 kHz with a relative size of 0.16 and the second around 5 kHz with a relative size of 0.21, the latter is of interest in the following.

3 The finite plate

We create a finite plate consisting of 10×10 base cells ($\approx34\times29$ cm) using the base cell in Fig. 4 (right). However, instead of choosing a rhombic area, we choose a rectangular area to secure equal stiffnesses at the four corners of the plate. We position a harmonic distributed load at the center of the plate to model the shaker that will be used to generate vibrations in the experimental study. The area of contact is circular with a radius of 6 mm. This is a simple model of the shaker used in the actual experiment and is described below. The accelerometer used in the experiment to measure the acceleration at a given position on the plate is modeled by a massless point gauge, which simply picks out the vibrational amplitude at a given point. In a numerical study, this simple model gave the same results as a model including mass and area of contact of the accelerometer due to negligible actuator weight compared to structural weight. In the investigations described below, the accelerometer is used to measure accelerations at different positions for a fixed frequency and to measure the accelerations at a fixed position for a range of frequencies. The plate with the area of contact of the harmonic load is shown in Fig. 6. We consider free boundary conditions for the finite plate because these are easiest to realize in the experiment. The finite plate is modeled using the following steady-state equation with circular frequency ω

$$(\mathbf{K} - \omega^2\mathbf{M} + \mathrm{i}\omega\mathbf{C})\mathbf{u} = \mathbf{f}_0 \tag{10}$$

where $\mathbf{f}_0$ is the amplitude of the distributed harmonic load. $\mathbf{K}$ and $\mathbf{M}$ are again the stiffness matrix and mass matrix; however, they differ in form and content from those of (5). $\mathbf{C}$ is a structural damping matrix. We did not perform a rigorous damping analysis. However, when calculating the acceleration frequency response function (FRF) in the following, we use damping to remove peaks in the frequency regime

$$\mathbf{C} = \frac{\beta}{\omega}\mathbf{K} \tag{11}$$

and use the constant of proportionality $\beta = 0.01$. The choice β for the theoretical frequency plot was the result of a small parameter study giving the best overall agreement with the experimental frequency response. In the FE analysis of the finite periodic plate, we use 21,500 triangular first-order elements.

The first question to be answered is how large the finite plate must be in order for finite size effects to be neglected from the boundaries. We investigate this by considering the harmonic load vibrating at a frequency of f=5 kHz, which is in the second band gap. We therefore expect an exponential decay of the vibrational amplitudes away from the load. We then monitor the vibrational amplitudes away from the load for different sizes of the finite plate. Let n denote the number of base cell lengths from the center of the plate to the edge along the horizontal direction (such that the distance between opposite vertical edges is $2n$). We then consider plates with $n = 1, 2, 3, 4$, and 5. The result is shown in Fig. 7. The positions of the nodes of the plate are illustrated in gray along the x-axis. Visual inspection reveals that the band gap

Table 1 Material parameters

Material	ρ (kg/m^3)	E (GPa)	ν
PolyCarbonate	1,200	2.3	0.35
Weak material	12	0.0023	0.35

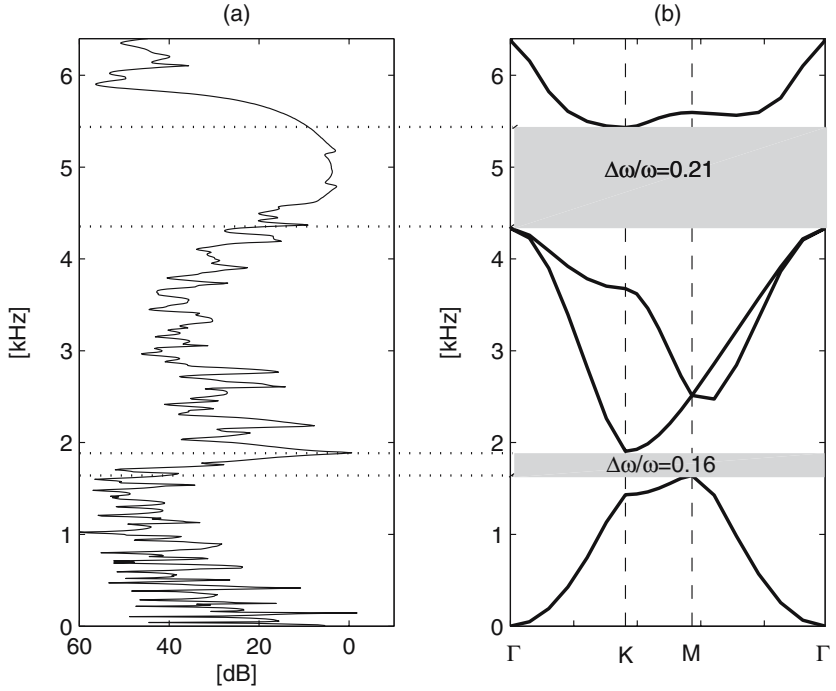

Fig. 5 **a** The acceleration plot for the finite plate in Fig. 6 calculated at the node with a horizontal distance of four base cell lengths from the center. **b** The dispersion plot for the infinite periodic plate with base cell shown in Fig. 4

effect is not present for plates with center-to-edge distances $n = 1, 2$, while the plates with $n = 3, 4$, and 5 seem to be sufficiently large for the effect to be present. The positions of the plate nodes suggest that the length of a base cell corresponds to half a wavelength for this band gap frequency. The dimensions of the plate should therefore be larger than three times the wavelength for a harmonic load placed at the center. This observation, together with the fact that a larger plate is preferable experimentally (to make it less sensitive to error sources), has lead to the choice of a finite plate with size $2n = 10$, see Fig. 6.

As a last point, the influence of the size of the plate on the FRF is shown in Fig. 8 for $2n = 10$ and 12. Here, the acceleration is shown as a function of frequency. The full line shows the acceleration for the 10×10 plate at the node placed four base cells away from the load along the horizontal direction. The dashed line and dotted-dashed line show the acceleration for a 12×12 plate at nodes four and five base cells, respectively, away from the load along the horizontal direction. This shows that the response drops significantly at the 5-kHz band gap when the distance to the load is increased while the distance to the edge is kept constant. A less pronounced drop is seen around the 2-kHz band gap. On the other hand, keeping the distance to the load constant while increasing the distance to the edge does not significantly change the response.

The acceleration plot for the 10×10 plate is compared with the dispersion plot for the corresponding infinite plate in Fig. 5. The acceleration plot was calculated at the node with a horizontal distance of four base cell lengths from the center. It is seen that the widths and positions of the band gaps for the infinite plate roughly show up as drops in the FRF plot for the finite plate (illustrated with horizontal lines). The drop at 2 kHz is around 35 dB while the drop at 5 kHz is around 25 dB. Discrepancies due to edge modes in the finite plate could possibly be removed by optimization.

The band gap effect is illustrated in Fig. 9 (left) showing the plate vibrations at a frequency f=5 kHz in the band gap.

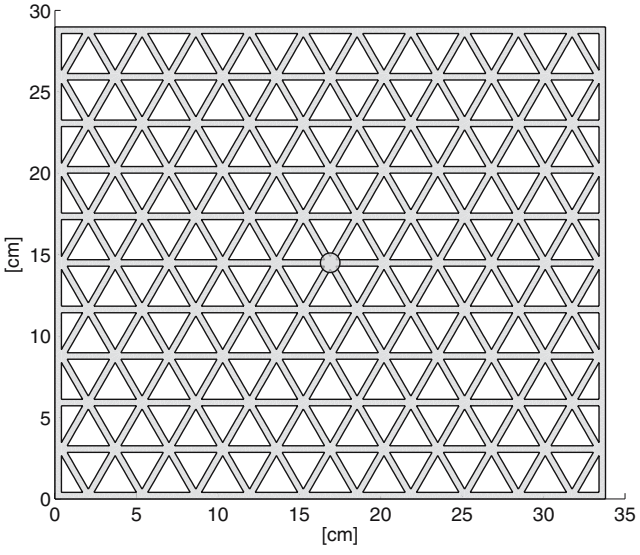

Fig. 6 The finite periodic plate consisting of 10×10 base cells. The harmonic load is shown at the center of the plate

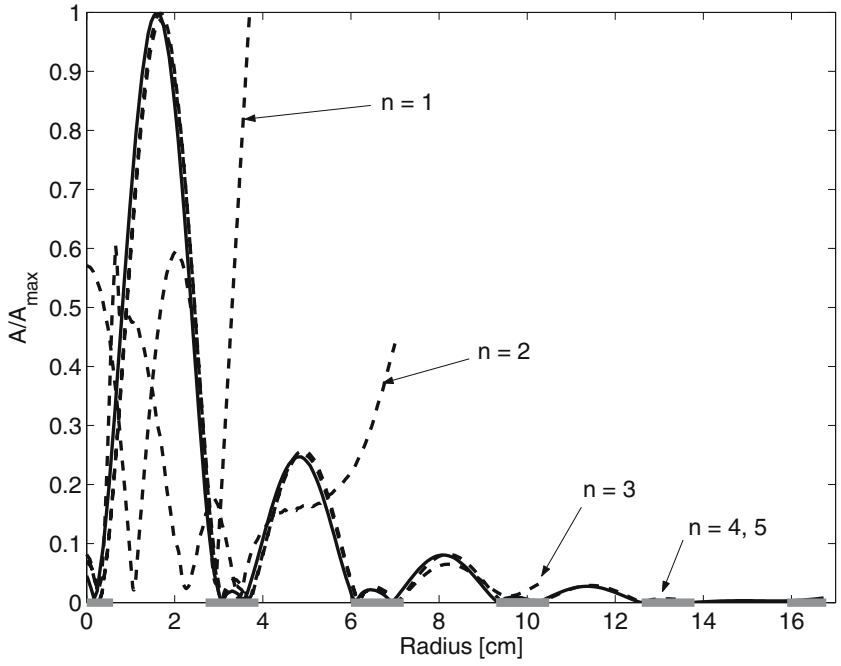

Fig. 7 Vibrational amplitudes as a function of horizontal distance from the harmonic load, f=5 kHz, for different sizes of the finite periodic plate. n denotes the distance in base cells from the *center* to the *edge* of the plate. *Gray* areas indicate plate nodes

The strong decay away from the load is clearly seen. The contour plot of the plate vibrations (right) clearly shows that the vibrations at the plate nodes are small while they are large between the nodes resulting in "localized" beams vibrating in the fundamental mode. From this it is hypothesized that a lower band gap may be created when the wavelength is approximately equal to twice the base cell dimensions (this is also known in optics).

As a contrast, Fig. 10 shows the plate vibrations at a frequency f=3 kHz outside the band gap. No decay is seen in this case and the contour plot shows vibrations also at the plate nodes in this case.

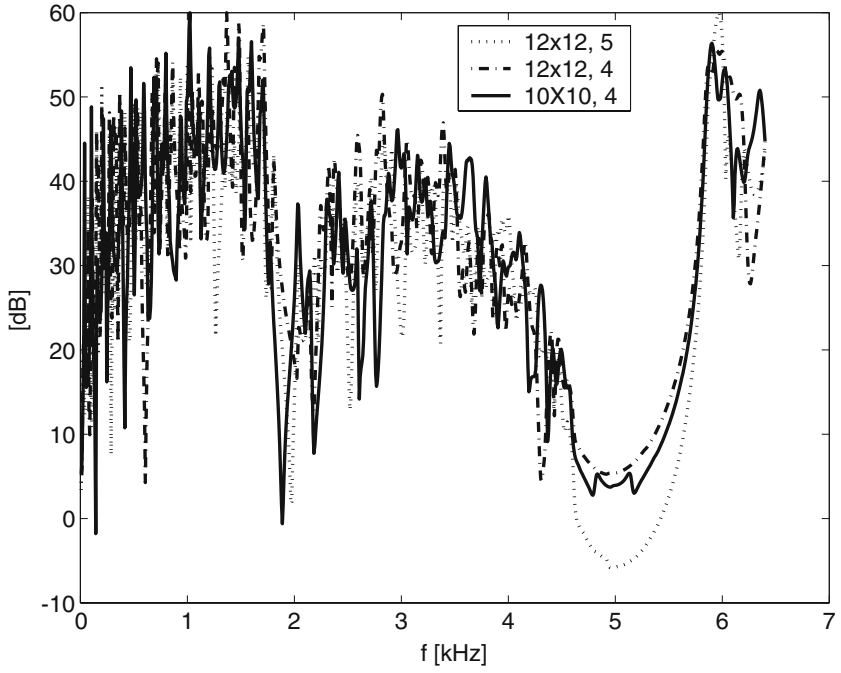

Fig. 8 The finite periodic plate. Acceleration plots for 10×10 and 12×12 plates showing the acceleration at different distances from the load (given in number of base cells) along the horizontal direction

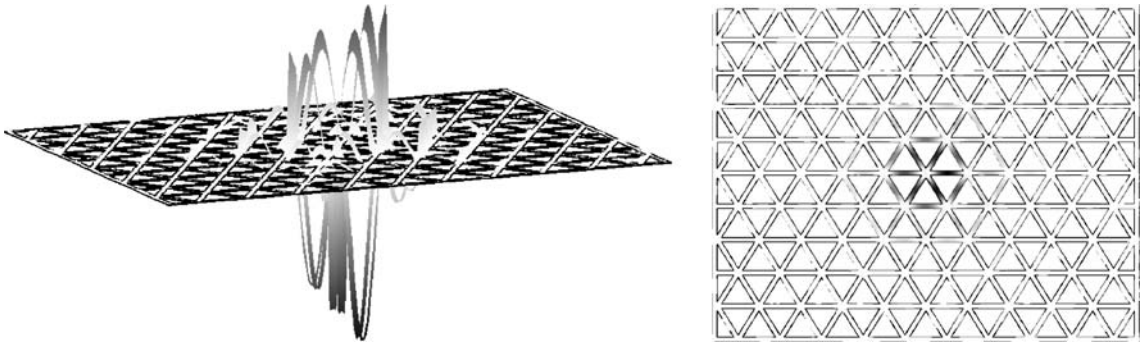

Fig. 9 *Sideview* and *contour plot* of the finite periodic plate structure showing the vibrations due to a harmonic load at a frequency f=5 kHz in the second band gap

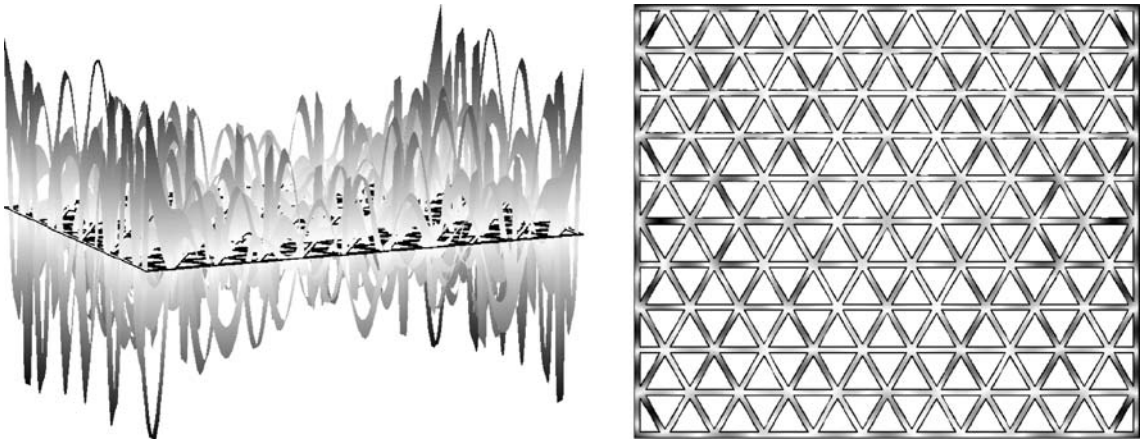

Fig. 10 *Sideview* and *contour plot* of the finite periodic plate structure showing the vibrations due to a harmonic load at a frequency f=3 kHz outside a band gap

4 Experimental investigation

The finite periodic plate was fabricated and an experimental investigation was carried out with the purpose of verifying the existence of the band gap effect in the fabricated plate. In accordance with the model description in the previous section we did not attempt to obtain a quantitative agreement. In the following, we therefore consider normalized results except in the final frequency response plot.

It was not possible to fabricate a plate with sharp triangular corners because the voids were milled using a tool with a radius of 1.5 mm, but only small discrepancies between the numerical and experimental results are expected due to this.

The plate material is PolyCarbonate (material parameters listed in Table 1). Figure 11 shows the fabricated periodic plate. The weight of the periodic plate is 144 g. Figure 12 shows the experimental setup, while Fig. 13 illustrates the used hardware. The plates are placed horizontally with their center on the shaker. This is experimentally convenient, and a small experimental investigation showed no significant difference in the results for vertical and horizontal plates. A shaker was chosen to generate the two types of plate vibrations investigated: a random signal to determine the FRF and single-frequency signal for studying bending amplitudes. The random signal was chosen instead of a frequency sweep, as it ensures a more uniform energy distribution over frequencies.

Plate vibrations are detected with an Endevco 22 accelerometer with a weight of 0.14 g. The vibrations are generated with a Brüel & Kjær Mini-Shaker 4810 using a Brüel

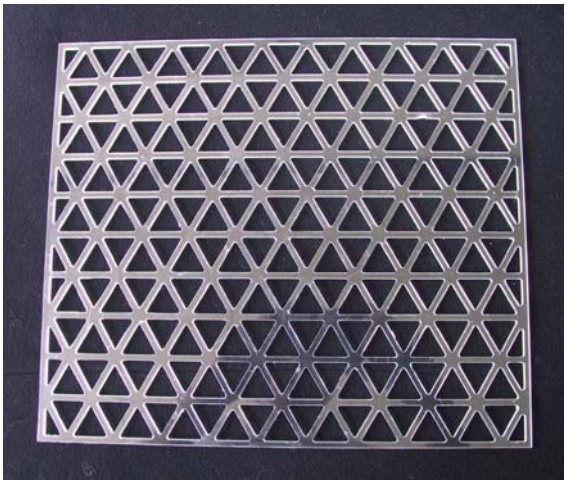

Fig. 11 The fabricated periodic plate made of PolyCarbonate consisting of 10×10 base cells

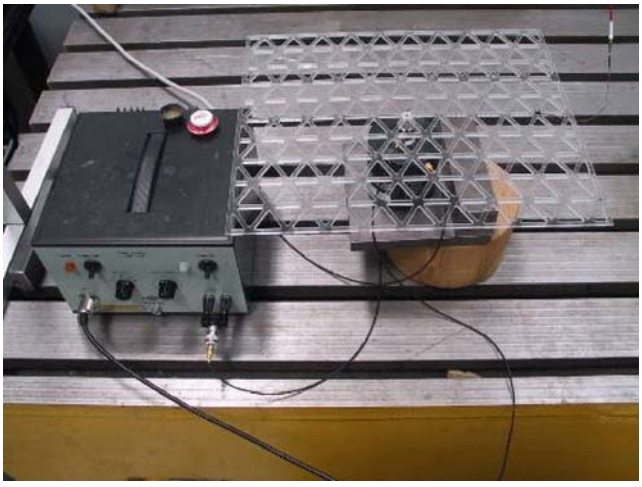

Fig. 12 Experimental setup

& Kjær power amplifier 2706. The area of contact between the shaker and the plate is of a circular shape with a radius of 6 mm. A thin wax layer is used to ensure proper attachment of the plate to the shaker. The shaker (power amplifier) and accelerometer are connected to the Brüel & Kjær PULSE platform consisting of a 3560 C frontend and PC software.

5 Numerical and experimental comparisons

This section is devoted to the comparisons between theoretical and experimental results. Figures 14 and 15 show the normalized vibrational amplitudes along the horizontal direction from the shaker at the center to the edge of the plate for two frequencies f=1.9 and 5 kHz, respectively, one in each band gap. The position of the plate nodes are shown along the x-axis. There is good agreement between the experimental and theoretical results and they clearly show the expected exponential decay of the amplitudes away from the shaker. Edge effects only show up quite close to the edge and somewhat more for the lower of the two frequencies.

Figure 16 shows the normalized amplitudes for a frequency f=3 kHz outside the band gaps. As expected, no exponential decay is seen for the amplitudes. The agreement between the experimental and theoretical results is not as good in this case, especially close to the shaker. It seems like more modes are present in the theoretical case than in the experimental case. A theoretical parameter study showed that the generation of modes is highly sensitive to the placement of the load within millimeters. The figure shows the best result comparative from a number of different load positions in the theoretical model.

The discrepancies between theoretical and experimental results near the shaker may also be attributed to the modeling of the shaker. The shaker is only modeled as a distributed load, which means we did not take into account the effect of the wax, which to some extent prevents local bending at the area of contact. This effect is expected to increase with increasing frequency.

Figure 16 does not reveal any significant exponential decay of the experimentally measured amplitudes, which could then be attributed to material damping as we are outside a band gap. Together with Figs. 14 and 15, this confirms that material damping is negligible in comparison with the band gap effect.

Finally, theoretical and experimental acceleration curves are shown in Fig. 17. These were measured at a horizontal distance of four base cell lengths from the center (see Fig. 12). There is reasonable agreement between the theoretical and experimental drop around 2 kHz ($\approx$ 30 dB) in width and height, while for the drop around 5 kHz ($\approx$ 25 dB), the experimental drop is much more narrow.

6 A corner supported plate

In the previous sections we have considered a finite periodic structure with free boundary conditions subjected to a harmonic massless load. This was done for experimental rea-

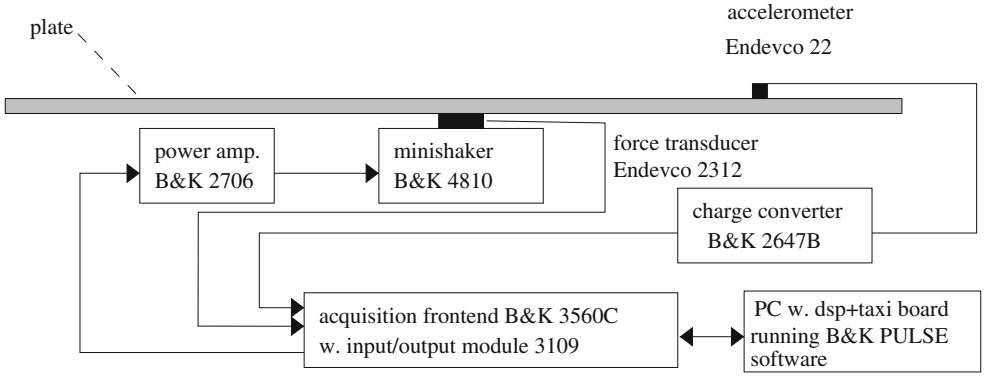

Fig. 13 Illustration of the used hardware

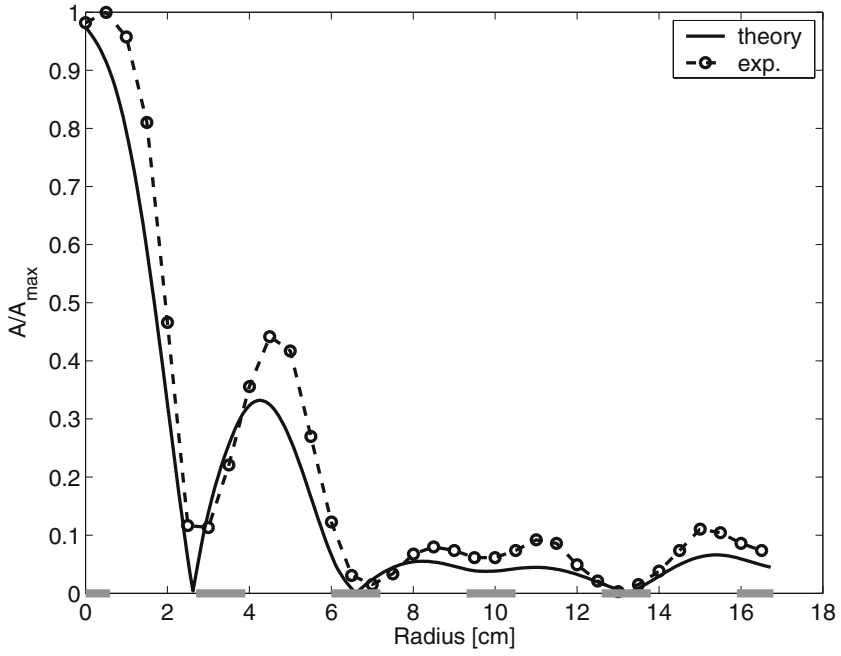

Fig. 14 The finite periodic plate. Experimental and theoretical normalized amplitudes along the horizontal direction from the shaker to the edge of the plate for a frequency f=1.9 kHz in the band gap

sons. However, in an actual application the structure would, e.g., be simply supported (zero displacements) at the four corners with the purpose of supporting a vibrating object with nonzero mass. Of practical interest would then be the reaction forces at these supports. The reaction forces should ideally be small in order not to transfer the vibrations to the surroundings. In the following, we therefore numerically study the size of these reaction forces incorporating the mass of the vibrating object.

The area of contact of the vibrating object is circular with a radius of one unit base cell and with center at the center of the structure. The mass of the object is set to ten times the mass of the perforated structure. The mass of the object is modeled by including it in the mass density of the part

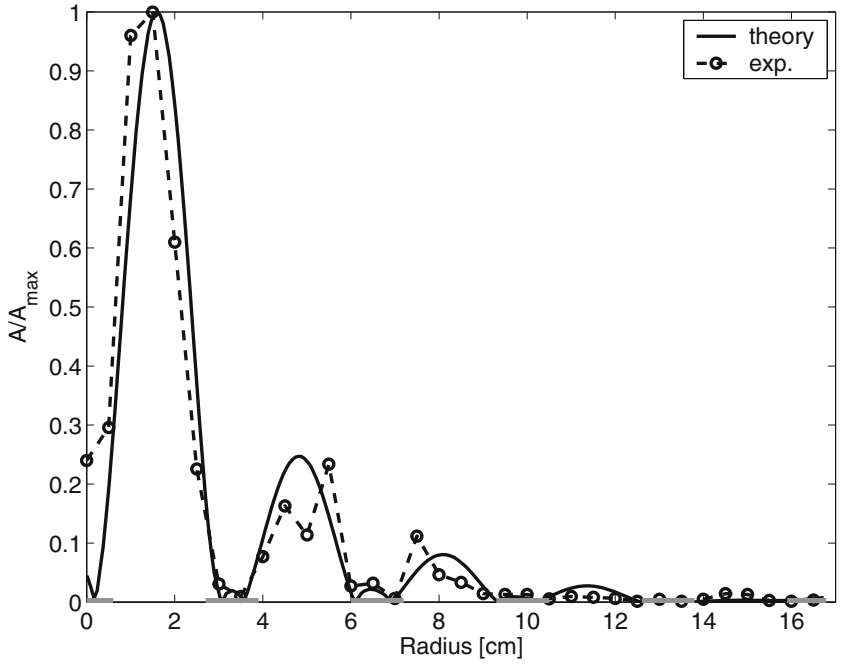

Fig. 15 The finite periodic plate structure. Experimental and theoretical normalized amplitudes along the horizontal direction from the shaker to the edge of the plate for a frequency f=5 kHz in the band gap

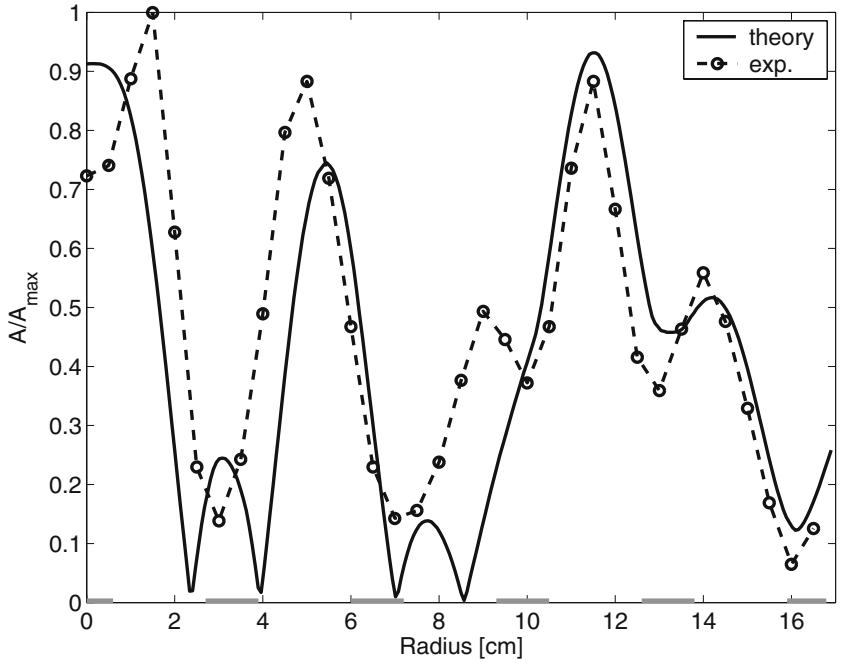

Fig. 16 The finite periodic plate structure. Experimental and theoretical normalized amplitudes along the horizontal direction from the shaker to the edge of the plate for a frequency f=3 kHz outside the band gaps

of the structure below the area of contact. The vibrations of the object is modeled with a harmonic vertical force acting uniformly over the area of contact

$$f(t) = f_0 \sin(\omega t)$$

We include the same damping (11) for the acceleration plots. For the simply supported plate, four reaction forces R_i are then calculated. We compute the sum of the absolute values of these forces $R = \sum_i |R_i|$, which takes rotary effects (antisymmetric modes) into account. The result is shown in Fig. 18 (full line), normalized with respect

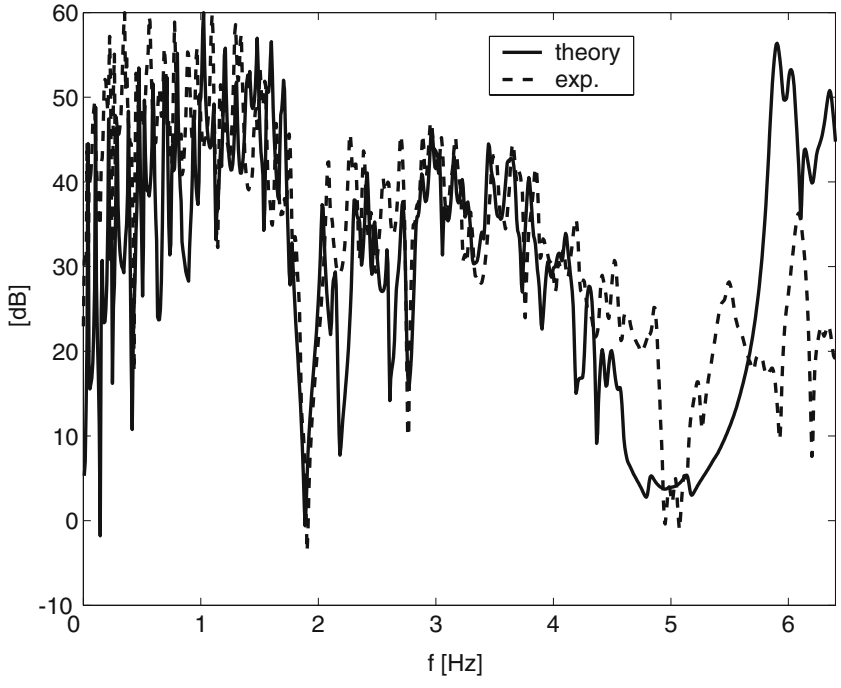

Fig. 17 The finite periodic plate structure. Experimental and theoretical acceleration plots

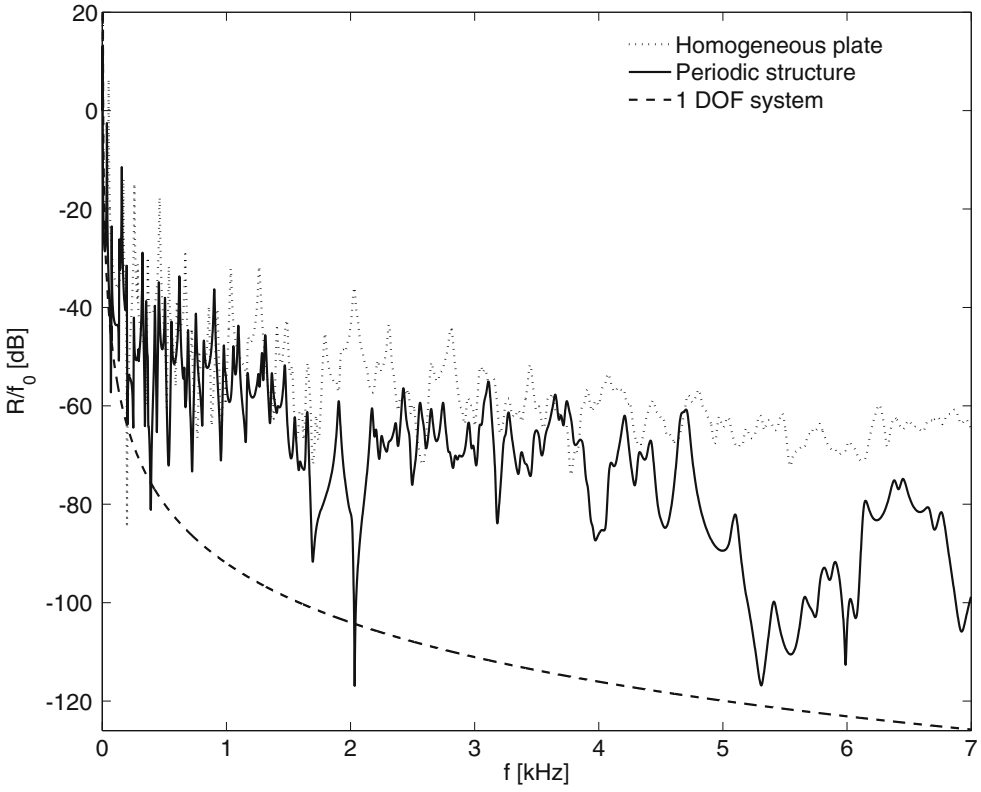

Fig. 18 Reaction forces for the simply supported plate. *Full line* represents the periodic structure while the *dotted line* represents the homogeneous plate

to f_0 and expressed in decibels. Two drops are seen at 2 kHz (depth 50 dB) and 5 kHz (depth 30–50 dB). Thus, the reaction forces are relatively small at frequencies in the band gaps as expected. Peaks within the drops are the results of edge modes.

We have investigated the same scenario for a homogeneous plate with the same dimensions and with the mass of the vibrating object the same as before. This was done to confirm that the designed structure is superior to the (conventional) homogeneous plate regarding vibration isolation in a practical situation. The result is also shown on Fig. 18 (dotted line). In this case, no similar drops in reaction forces are seen at frequencies in the band gap intervals.

For comparison we also added the response of a 1-degree-of-freedom system with the same fundamental eigenfrequency as the homogeneous plate with added mass. The response of our perforated plate is generally higher due to the multitude of modes; but especially in the frequency range around the second band gap near 5 kHz, the response of the plate approaches that of the spring, which in this respect can be viewed as the idealized vibration isolator.

7 Conclusions

Using topology optimization, we have designed a base cell in an infinite periodic plate with a maximized frequency band gap size. Interpretation and postprocessing of the topology optimized base cell design were carried out to achieve a final structural design with better robustness properties and which is possible to fabricate using conventional equipment. Of course, this is achieved at the cost of smaller band gap properties. Using this final base cell design, we have designed a finite periodic plate and we have shown how the band gap effect present in the infinite periodic plate may be transferred to the finite plate subjected to a centered harmonic load with a frequency in the band gap, provided that the dimensions of the plate are at least a few ($\approx$3) wavelengths. An interpretation was attempted to explain the position of the band gap relative to the size of the base cells and the physics of the phenomenon.

The designed plate was fabricated using conventional milling equipment and experimental investigations were carried out. In general, the theoretical and experimental results show good agreement, verifying the existence of the band gap effect in the fabricated plate.

A practical scenario with the periodic structure simply supported at its corners and subjected to a vibrating object with a mass was modeled and investigated. As expected, the reaction forces experience drops at frequencies in the band gaps. Thus, it is believed that the periodic structure can be useful in practical situations where minimization of the vibrations transferred to the surroundings is an issue.

Future work includes optimization of the finite periodic plate itself, and also including the boundaries. Finally, the topic of the optimal base cell geometry needs further study.

Acknowledgements This work was supported by Denmark's Technical Research Council (project title "Designing bandgap materials and structures with optimized dynamic properties") and the Eurohorcs/ESF European Young Investigator Award (EURYI) (project title "Synthesis and topology optimization of optomechanical systems").

References

Bendsøe MP, Sigmund O (2003) Topology optimization—theory, methods and applications. Springer, Berlin Heidelberg New York

Borel PI, Harpøth A, Frandsen LH, Jensen M, Jensen JS, Sigmund O (2004) Topology optimization and fabrication of photonic crystal structures. Opt Express 12:1996–2001

Borrvall T, Petersson J (2001) Topology optimization using regularized intermediate density control. Comput Methods Appl Mech Eng 190:4911–4928

Cox SJ, Dobson DC (1999) Maximizing band gaps in two-dimensional photonic crystals. SIAM J Appl Math 59(6):2108–2120

Diaz AR, Haddow AG, Ma L (2005) Design of band-gap grid structures. Struct Multidisc Optim 29(6):418–431

Graff KF (1991) Wave motion in elastic solids. Dover, Boulder, CO

Halkjær S, Sigmund O, Jensen JS (2005) Inverse design of phononic crystals by topology optimization. Z Kristallogr 220(9–10):895–905

Jensen JS, Sigmund O (2004) Systematic design of photonic crystal structures using topology optimization: low-loss waveguide bends. Appl Phys Lett 84:2002–2024

Kao CY, Osher S, Yablonovitch E (2005) Maximizing band gaps in two-dimensional photonic crystals by using level set methods. Appl Phys B Lasers Opt 81(2):235–244

Leissa A (1993) Vibration of plates. Acoustical Society of America, Melville, NY

Matthews J, Walker R (1964) Mathematical methods of physics. Addison-Wesley, USA

Mindlin RD (1951) Influence of rotary inertia and shear on flexural motions of isotropic, elastic plates. J Appl Mech 18:31–38

Sigalas MM, Economou EN (1994) Elastic waves in plates with periodically placed inclusions. J Appl Phys 75(6):2845–2850

Sigalas M, Kushwaha MS, Economou EN, Kafesaki M, Psarabas I, Steurer W (2005) Classical vibrational modes in phononic lattices: theory and experiment. Z Kristallogr 220(9–10):765–809

Sigmund O, Jensen JS (2003) Systematic design of photonic band-gap materials and structures by topology optimization. Philos Trans R Soc Lond A 361:1001–1019

Svanberg K (1987) The method of moving asymptotes: a new method for structural optimization. Int J Numer Methods Eng 24:359–373